AIAA 79-1718R

On-Orbit Control System Performance of the HEAO-2 Observatory

R.E. Rose* and E.A. Berkery†
TRW Defense and Space Systems Group, Redondo Beach, Calif.

The on-orbit performance of the High Energy Astronomy Observatory is described. The control system utilizes precision gyros for attitude reference and skewed reaction wheels controlled by a reprogrammable computer. The observatory points at selected targets, maneuvers automatically, and acquires guide stars for updating at each target. Performance data indicate maneuver accuracies less than 1 arc-min and pointing accuracies of 2-5 arc-sec. Use of 7th to 9th magnitude guide stars has resulted in several improper updates caused by "flat-field" stray light effects in the star trackers. The method used to discriminate true stars from the flat-field is also presented.

Introduction

NASA's second High Energy Astronomy Observatory (HEAO-2) was successfully inserted into orbit on Nov. 13, 1978. Carrying the largest focusing x-ray telescope ever flown and a variety of sophisticated sensitive detectors, HEAO-2 has been designed to maneuver and point for long periods of time at selected celestial x-ray sources, some of which were only recently discovered by its scanning predecessor, HEAO-1. The data being returned by HEAO-2 includes the first spacecraft-generated high-resolution x-ray images of celestial objects other than the sun. Precise pointing and high stability are required during the imaging process.

The development program for the three HEAO scientific observatories was initiated in July 1974. Each of the three spacecraft contains a unique complement of scientific experiments selected to support the program objective of x-ray, γ-ray, and cosmic-ray astronomy.

The three HEAO spacecraft have a common basic control system design, but because of widely differing mission goals, significant differences exist in control requirements. Additional information on the design concepts are found in Refs. 1 and 2. HEAO-1 and HEAO-3 are scanning missions with reaction control systems (RCS) capable of 1 deg orientation accuracy and 0.1 deg attitude determination accuracy. HEAO-2 is a precision pointing mission requiring 1 arc-min pointing and 1 arc-sec/s stability.

To date, HEAO-2 has completed one year of operation and has produced more than 1000 images including the brightest, most distant, and most powerful objects yet observed to emit x-rays—quasars estimated to be more than 10^{10} light years from Earth. The intense energy from quasars, strange starlike objects that radiate inordinate amounts of energy for their apparently small size, suggests that they may contribute significantly to the widespread low-level background of cosmic x-ray radiation detected. This discovery could leave important implications for theories of cosmic evolution, for it would mean that the proposed mass necessary to "close" the universe is not present in the form of hot gas and, indeed, may be missing.

This paper highlights the performance characteristics of the HEAO-2 spacecraft control system to achieve the required accuracy. Correlation with preflight predictions of servo performance and disturbance torques was performed for HEAO-1 in Ref. 3 and is, therefore, not discussed. The achieved on-orbit performance is described for maneuvering, automatic acquisition of targets, and long-term pointing. Data is given showing capabilities to perform eigenaxis maneuvers up to 180 deg and arrive at an accuracy typically less than 1 arc-min. Subsequent search for "guide stars" is automatically initiated. Discrimination logic used on-board to insure that the guide stars are correct is also described. Successfully passing these logic tests allows attitude reference updates and final pull-in to the desired target. Pointing performance data is also described indicating that pointing accuracies on the order of 2-5 arc-sec are achieved.

HEAO-2 General Description

The grazing-incidence x-ray telescope on HEAO-2 will produce images of x-ray sources which are then analyzed by any of four interchangeable instruments at the focal plane of the telescope. In addition to the instrument at the focal plane, there is one complementary instrument which directly views the areas out in space along the same direction as the telescope.

The science objectives of the HEAO-2 telescope experiment are:

1) Determine structural details of extended wide x-ray sources and identify with optical objectives by studying x-ray images.

2) Perform spectroscopy measurements to determine x-ray emission mechanism and spectral features.

3) Analyze temporal behavior of x-ray sources on a scale from 1 μs to 1 yr.

HEAO-2 instruments are the monitor proportional counter, high resolution imager, focal plane crystal spectrometer, imaging proportional counter, solid-state spectrometer, the broad band filter spectrometer, and the objective grating spectrometer, as shown in Fig. 1.

The various instruments were physically and functionally integrated into a telescope experiment configuration by American Science and Engineering, which was subsequently calibrated in the new X-Ray Test Calibration Facility at Marshall Space Flight Center (MSFC). The assembled telescope was delivered from MSFC to TRW for integration with the spacecraft module and the spacecraft structure.

Some of the general features of the observatory are shown in Table 1. The experiments all view out along the $+x$ axis of the observatory. The $+z$ axis, normal to the solar array, is maintained within a 15 deg cone of the sun (power and thermal constraint) during normal operation. Within this constraint the observatory maneuvers up to two maneuvers per orbit. The design requirements for the attitude control and

Presented as Paper 79-1718 at the AIAA Guidance and Control Conference, Boulder, Colo., Aug. 6-8, 1979; submitted Nov. 2, 1979; revision received July 14, 1980. Copyright © American Institute of Aeronautics and Astronautics, Inc., 1979. All rights reserved.

*Senior Staff Engineer, Control and Sensor Systems Laboratory. Member AIAA.

†HEAO Attitude Control Subsystem Operations Engineer, Greenbelt, Md.

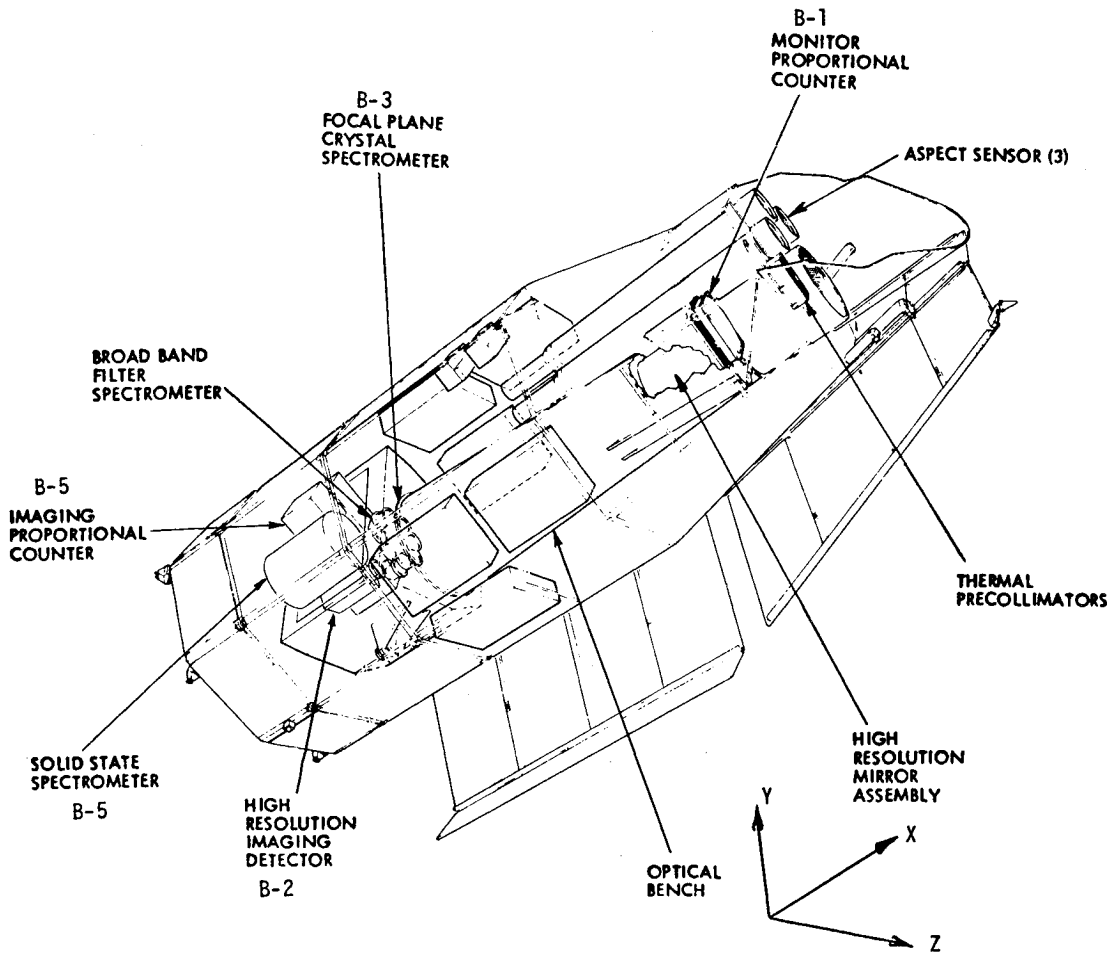

Fig. 1 HEAO-2 experiments.

Table 1 General features of HEAO-2

Physical	
Size	22.4 ft high × 9 ft diam
Weight	6869 lb
Inertia	$I_{xx} = 1492$ $I_{yy} = 8458$ $I_{zz} = 8502$
Orbit	
Altitude	290 n.mi.
Inclination	23.5 deg
Eccentricity	0 (circular)
Subsystems	
Power	565 W
Command	8/s
Telemetry	6.4K bits/s
RCS	300 lb hydrazine 12-1 lb_f thrusters
Star trackers (3)	2 deg × 2 deg FOV 2-9th magnitude stars accuracy = 1.5 arc-sec, calibrated
Reaction wheels (4)	30 ft-lb-s momentum (each)

determination subsystem (ACDS) to perform the mission objectives are summarized in Table 2. The performance capabilities demonstrated to date by on-orbit experience indicate that all requirements are being met and exceeded.

ACDS Design Description

The HEAO-2 ACDS was designed to utilize maximum commonality with the other two observatories in the series, HEAO-1 and HEAO-3. The design, therefore, reflects not only the design requirements of Table 2 but also those items common with the mission goals of HEAO-1 and HEAO-C. The differences between these missions were accommodated in HEAO-2 hardware by the addition of four reaction wheels and replacement of the 1/3 star trackers with the three HEAO-2 experiment star trackers. All other changes are performed in the flight program software implemented in the flight computer.

The control system block diagram is shown in Fig. 2 and the equipment locations are shown in Fig. 3. The central element of the control system is the transfer assembly which accepts signals from all sensors and distributes commands to the actuators. The digital processor assembly processes all sensor inputs, implements control laws and logic, accepts, processes, and distributes commands, and outputs telemetry. References 3 and 4 provide a more detailed description of the ACDS components. The RCS thrusters are 1 lb NASA standard used for the "safe" mode, normal sun acquisition, and for momentum desaturation of the reaction wheels. The four reaction wheels each provide storage of 30 ft-lb-s of momentum and produce 25-50 in.-oz of torque. The wheels are mounted in a skewed configuration (square base pyramid) such that any three will provide three-axis control, with all four wheels used for normal operation. Sun sensors on the $\pm y$ and $\pm z$ faces of the spacecraft provide 4π coverage for acquisition and include a z axis fine sun sensor. The six gyros are mounted in a dodecahedron configuration, such that any three provide three-axis information. The precision gyros are gas bearing, pulse rebalanced rate integrating devices having 0.1 arc-sec quantization and an advertised drift rate of 0.003 deg/h, 1σ, and 20 ppm nonlinearity. The three-star trackers have a 2 × 2 deg field of view (FOV), can detect 9th magnitude

stars, and have an advertised accuracy of 1.5 arc-sec calibrated.

During all normal operations, a precision onboard attitude reference is maintained in the digital processor by propagation of the Euler symmetric parameters (also referred to as the reference quaternion) using gyro data. In the celestial point mode of operation, the reference is updated by star tracker data using the pseudoinverse technique of Ref. 3.

The control system modes include: 1) standby, 2) normal sun acquisition (NSA), 4) celestial point (CP), 5) momentum desaturation, 6) maneuver, and 7) star acquisition. Celestial scan (mode 3) is used on HEAO-1 and HEAO-3 only. In addition to these, a "safe" mode is provided which allows sun acquisition with minimum equipment (circumvents star trackers, wheels, flight computer, gyros, and most of the transfer assembly such that no normal mode hardware is common). This safe mode uses only redundant sun sensors and thrusters plus hardwired logic in the transfer assembly described in Ref. 3. In the safe mode, the spacecraft is allowed to drift during eclipse with automatic sun reacquisition at dawn. In the normal sun acquisition mode, control is provided by RCS thrusters, using sun sensors for position in sunlight, gyros for rate feedback, and (integrated rate) position in eclipse. HEAO-2 has used the normal sun acquisition mode only once, at spacecraft separation from the Centaur launch vehicle. Since the Centaur places the observatory with the $+z$ axis toward the sun prior to separation, the total acquisition angle of the observatory was less than 6 deg. The functional requirement of the celestial point mode is to orient the telescope optical axis ($+x$ axis) to celestial targets of interest for periods of a few minutes to several orbits. The targets are specified by the ground control center based on a preplanned scenario. The target sequence requires target-to-target maneuvering.

The star tracker orientationwwere selected to optimize their utility for the experiment since only accurate x axis pointing is of primary importance. Reduced accuracy is allowed for rotations about the x axis, since only the corners of the experiment FOV are affected. Rotational error about the x axis is only of importance for maneuvers. The star tracker orientations and the maneuver targeting concept are shown in Fig. 4. While pointing at a target, control is performed with reaction wheels using the gyro propagated reference. Each 74 s the star trackers are interrogated such that an update can be performed. The on-board logic requires that two "guide stars" be found, one in each of two preselected trackers and at predetermined locations within the error boxes as shown. The

Table 2 ACDS design requirements (left) and performance summary (right)

Functional	
Celestial point operation, maneuver to any orientation ± 180 deg	Over 1000 targets visited in first year of operation
Automatic star acquisition and on-board update	Operating successfully
Normal sun acquisition mode for recovery and attitude initialization	Sun acquisition mode used once—Nov. 13-15, 1978 at launch
Minimum-complexity safe mode for failure recovery and keep alive	Operated per plan at separation for 2 min prior to sun acquisition mode entry
Design	
12 month mission for expandable sizing and design life	100 lb of 300 lb available used in first year with momentum management
	One gyro of six has been lost due to thermal control failure
	One star tracker of three inoperable
Performance	
Pointing accuracy of 1 arc-min (0.68 CEP) in y and z	Target pointing 2-5 arc-sec for virtually all observations
Attitude determination accuracy of 1 arc-min (0.68 CEP)	Evidence shows <2 arc-sec
Maneuver accuracy better 75 arc-min^2 window	Maneuvers better than 1.5 arc-min^2
Jitter—not to exceed 1 arc-sec/s	Jitter not proven—experiment feedback indicates $\ll 1$ arc-sec/s

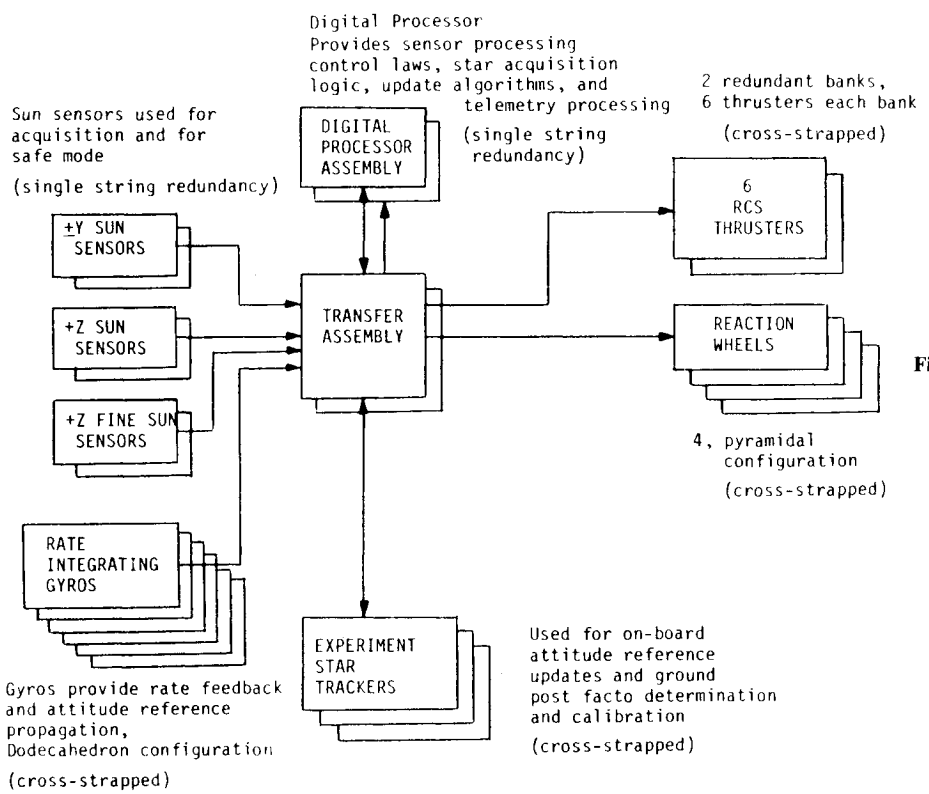

Fig. 2 HEAO-2 control system block diagram.

error boxes have been selected to be as large as possible, consistent with unambiguous guide stars as described in Ref. 5. These boxes are nominally 75 arc-min^2, typically 5 arc-min $\times$ 15 arc-min. Once the guide stars are found, their separation angle is checked as additional insurance that they are the correct stars. If this test is passed, the update is performed.

Maneuvers are performed using a "model" technique. Using the initial and final target orientations and the available momentum, an eigenaxis (maneuver axis) rotation is computed. The observatory then follows this rotation at a specified rate by following a steadily moving model. The model is shut off just prior to target arrival. Upon arrival within 0.4 deg, an integrator is introduced into the forward loop to eliminate hang-off error caused by the slowly varying disturbance torques. The control law is shown in Fig. 5. Maneuvers can be performed using either three or four wheels and with residual system momentum. During initial orbital operations, the three-wheel algorithms were proven during a brief period, switching to four-wheel operation for all subsequent pointing and maneuvering operations. With four wheels, a constraint law is required to achieve distribution of momentum. A specific portion of the available momentum must be reserved for accumulated momentum during the maneuver. Once target arrival has occurred (defined as a pointing reference error <0.015 deg and body rates less than 0.02 deg/s), guide star search is automatically initiated (star acquisition mode) and the tests are performed as described. After stars are acquired, the first update results in final acquisition and transition to steady-state celestial pointing.

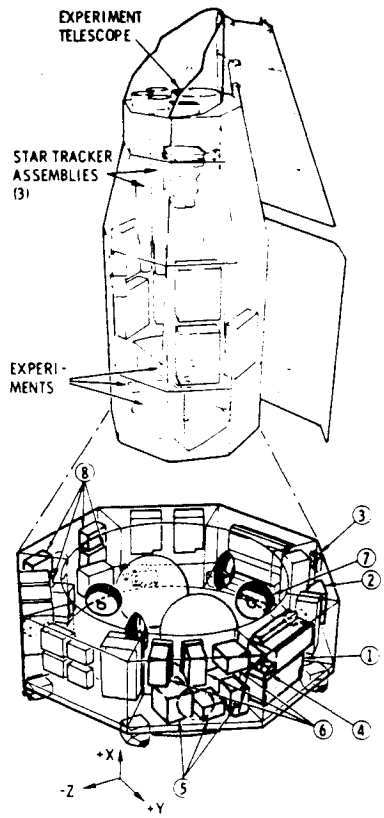

① TRANSFER ASSEMBLY (TA)
② DIGITAL PROCESSOR ASSEMBLY (DPA)
③ Z SUN SENSOR ASSEMBLY (ZSSA)
④ Y SUN SENSOR ASSEMBLY (YSSA)
⑤ RATE SENSOR UNIT (RSU)
⑥ ELECTRONICS CONTROL UNIT (ECU)
⑦ REACTION WHEEL ASSEMBLY (RWA)
⑧ REACTION WHEEL ELECTRONICS ASSEMBLY (RWEA)

Fig. 3 HEAO-2 configuration.

Operational Experience

The first week of on-orbit operation was utilized for checkout and calibration of the observatory. The planned targeting sequence allowed "fine tuning" corrections to gyro bias, alignment and scale factors, and detailed checkout of all observatory components and experiments. This sequence consisted of seven carefully selected transition pointing targets. A total of 21 maneuvers were performed between these targets to obtain calibration data. After completion of calibration, the science program was begun.

During the first five months of operation, over 500 pointing sequences were performed. The accuracy of pointing and maneuvering cannot be observed directly, but measurements can be combined to provide indications of the performance achieved.

Point Mode Performance

For science missions, the end product for ACDS is the accuracy and stability of the experiments. To this end, the experiments have obtained absolute accuracy less than 2 arc-sec. This accuracy is obtained by processing the star tracker output each minor frame (0.320 s), computing deviations from "nominal." Nominal is a major frame time solution (128 minor frames or 40.96 s) using gyro data to smooth the star tracker data within the frame. Gyro data is used only to propagate the solution to any time within the frame. The gyro data is used because the gyro short-term attitude noise is only 0.3 arc-sec (1σ), while worst-case star tracker noise can be as large as 1.5 arc-sec (1σ) for very dim (8-9 mV) guide stars. Experiment alignment relative to the star trackers is correlated periodically using "fiducial lights," which are introduced into the star trackers using optical "periscopes" from the experiment optical bench.

A convenient measure of pointing performance is given by the magnitude of the attitude reference update that is

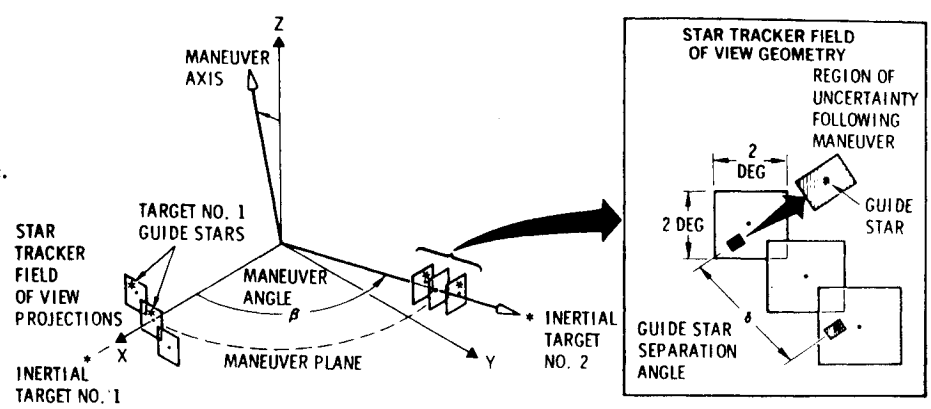

Fig. 4 HEAO-2 targeting concept schematic.

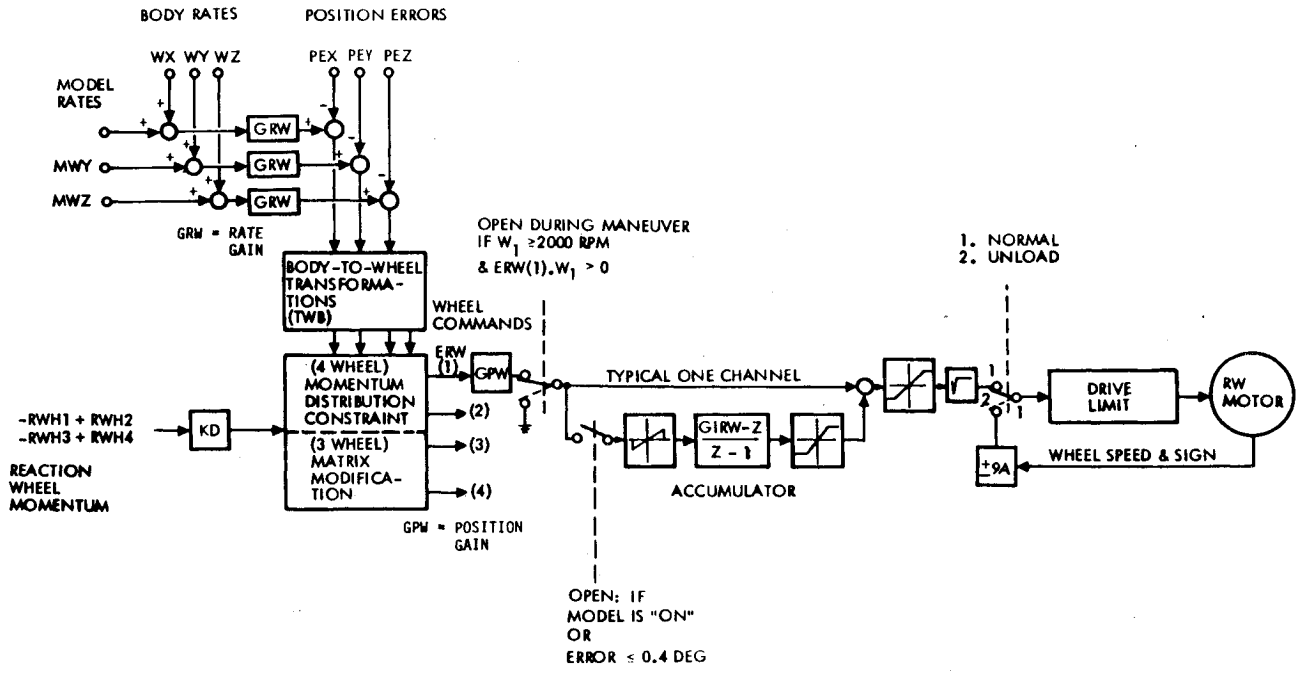

Fig. 5 Block diagram—HEAO-2 reaction wheel control system.

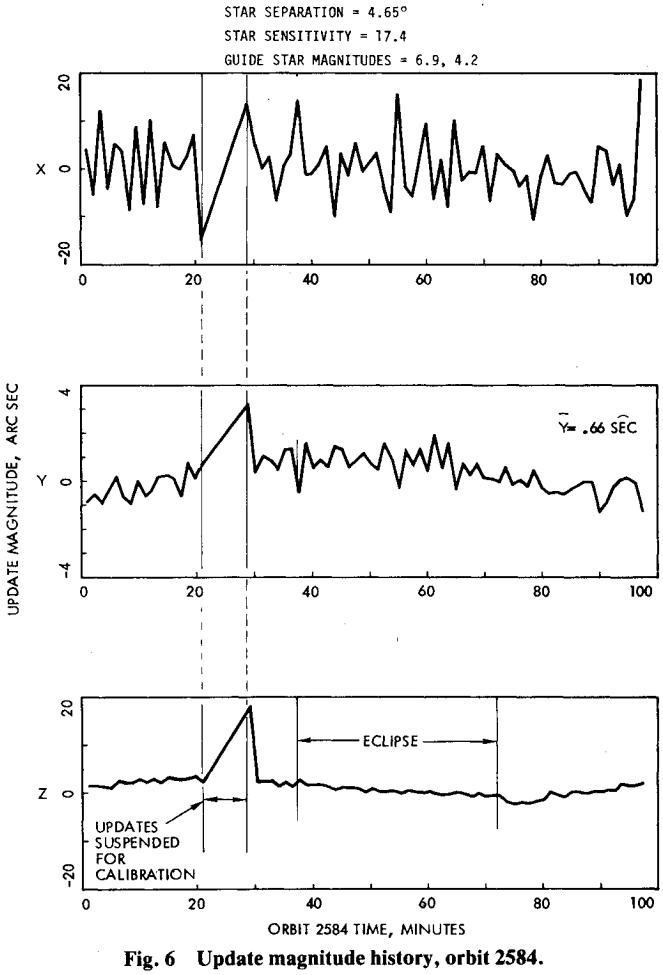

Fig. 6 Update magnitude history, orbit 2584.

nominally performed each 74 s. An entire orbit of update data is given in Fig. 6. Steady-state pointing occurred during the entire orbit, except for a 7-min period of suspended updates caused by a fiducial light calibration. The calibration excursion is indicative of uncompensated gyro bias. The update amplitudes in y and z have 0.62 and 1.28 arc-sec expected values, respectively. The sensitivity of x-axis error (expected value 5.3 arc-sec) to star separation varies inversely to star separation and has a value of 17.4 for the 4.6 deg separation of the guide stars. The x-axis pointing error is consistent with this sensitivity. Detailed examination of the data indicates that star tracker noise of one guide star (6.9 mV) is the dominant source of update-to-update variation. Since the reference update is a one-shot method (pseudoinverse), noise is transferred to the reference directly, filtered only by the combined geometry effects of the two guide stars.

It can be noted that the y and z update records of Fig. 6 show a slight sinusoidal characteristic at orbit rate, having a 0.7 arc-sec peak in y and a 1.8 arc-sec peak in z after extraction of fixed bias. This sinusoid is a systematic error source which causes updates in a given direction for half the orbit and the opposite direction for the other half. Three candidate contributors to this error have been identified:

1) Star aberration (due to orbital velocity) causes about 5.3 arc-sec (peak) with at least 70% of this worst case known to occur in this orbit.

2) Ground simulations of thermal bending have shown that distortion of the equipment compartment of up to 19 arc-sec is possible over worst-case orbits.

3) Gyro drift variation with bus voltage could account for the observed sinusoid with a change in uncompensated drift of 0.018 deg/h. Bus voltage variation of 6 V total occurred between sunlight and eclipse. The resulting required sensitivity of 0.003 deg/h-V is smaller than the actual measured gyro sensitivity of 0.005 deg/h-V. Gyro geometry effects also contribute sufficiently to account for the differences between the above sensitivities. These effects probably contribute to uncertainty in ground computation of gyro bias. A three-month history of the ground computed bias is shown in Fig. 7.

Star aberration is probably a minor contributor to the observed error. Since the remaining sources are both of reasonable values to account for the 0.7-1.8 arc-sec sinusoids, it has been presumed that both are contributors, but data obtained to date has not allowed separation of their individual contributions. None of these errors actually contribute to celestial pointing steady-state error with any significance, because pointing error is corrected by star tracker data each 74 s, and only the error accumulated between updates appears as a pointing error. Since these are less

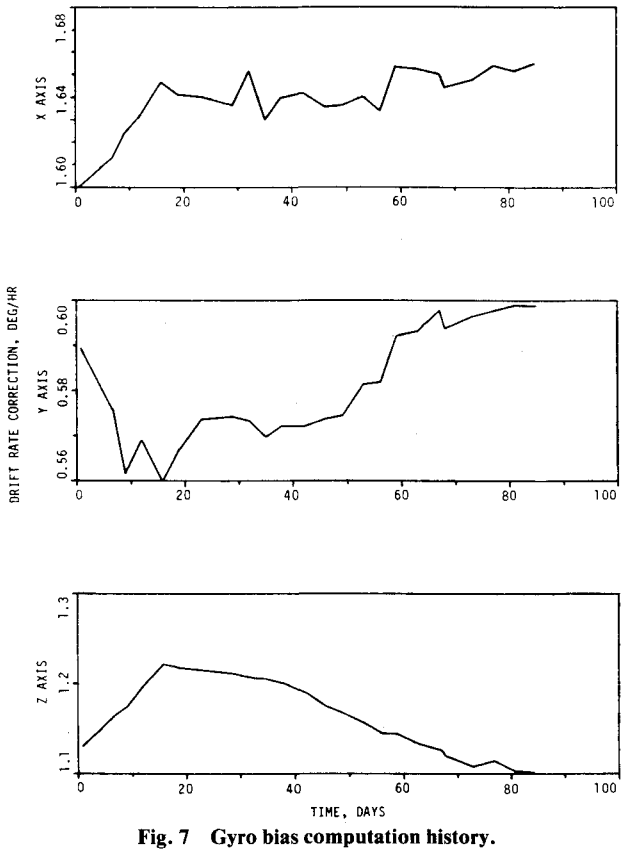

Fig. 7 Gyro bias computation history.

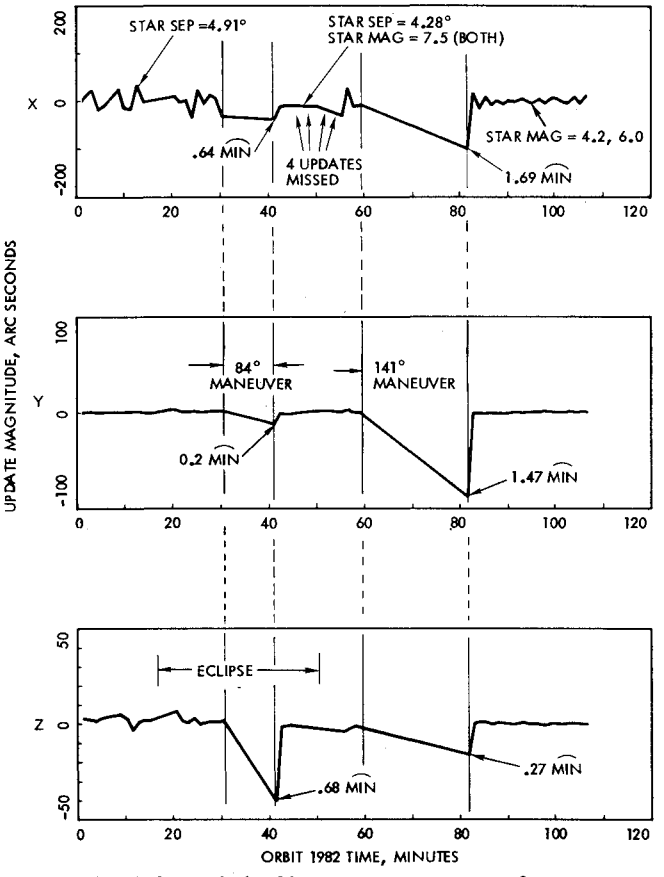

Fig. 8 Update pointing history, two-maneuver performance.

the tracker noise, the star tracker error is dominant. It is important to note that the star trackers and gyros are at opposite ends of the spacecraft. Very frequent updating holds the star trackers and the experiment on the stars as desired by the experiment. Perfect gyros, being inertial devices, would sense star aberration and spacecraft bending and introduce these motions into the attitude reference. The HEAO gyros have sensed these effects and thereby account for the apparent sinusoidal reference variations.

The update one-shot process does not contribute significantly to spacecraft jitter or pointing error because of the smoothing provided by reaction wheel response to the 1-2 arc-sec updates. This has been verified by the science investigators, stating that observed jitter and update motion is less than 0.2 arc-sec/s.

Maneuver Performance

Figure 8 shows the attitude reference update history for an orbit (orbit 1982) that contains two maneuvers: the first an 84 deg maneuver executed while in eclipse; the second, a 141 deg maneuver executed in sunlight. This figure shows error accumulations that occurred during each maneuver, since these errors are almost entirely equal to the magnitude of the first update after the maneuver. The maneuver (y,z) errors shown are 0.2, 0.68 arc-min for the 84-deg maneuver, and 1.47, 0.27 arc-min for the 141-deg maneuver.

It is interesting to note the change in error accumulation rate during each of the two maneuvers since one is performed in eclipse (when bus voltage is low), the other in sunlight. If the entire error is assumed to be caused by gyro bus voltage drift sensitivity, then the change in apparent drift between the two maneuvers is about 0.05 deg/h in each axis. Gyro configuration geometry is such that the z axis rate is determined by a single gyro. The equivalent change in gyro axes is 0.043 deg/h. A change of this magnitude for the orbit presented previously would be more than enough to account for the 0.7-1.8 arc-sec sinusoidal characteristic.

The maneuver errors for 50 maneuvers are shown in Fig. 9, plotted as separate points for each of the y- and z-axis errors.

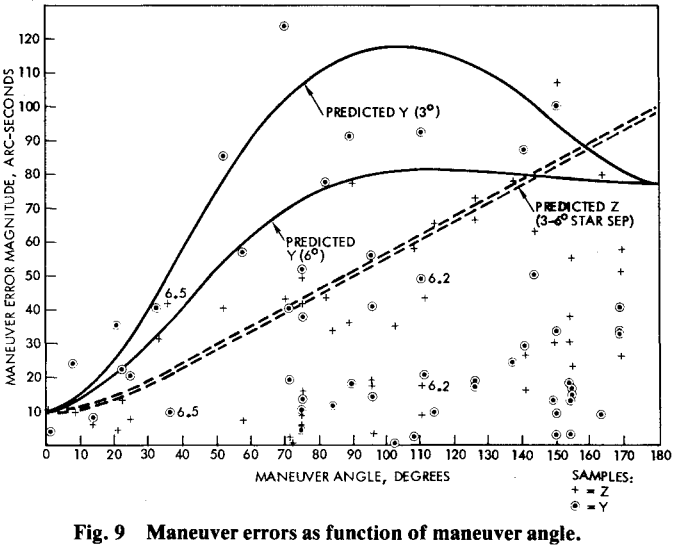

Fig. 9 Maneuver errors as function of maneuver angle.

Errors about the x axis at maneuver completion are negligible for star acquisition since the star trackers are all oriented within 2.5 deg of x. If treated as a single population, the maneuver errors are less than 41 arc-sec with probability 0.68, less than 82 arc-sec with probability 0.83, and less than 123 arc-sec with probability 0.99. The population, therefore, appears to be roughly normally distributed, with $1\sigma = 41$ arc-sec. However, there are known correlations between specific error sources and maneuver error magnitude in given axes when all maneuvers are performed about the same axis. This is true for HEAO-2, since most maneuvers are performed about the z axis, which, in turn, is generally in the direction of the sun. Errors of the z axis can be seen to have approximately a linear dependence on the maneuver angle, first because of scale factor error (proportional to angle), and second because

large uncompensated gyro bias errors will increase approximately with maneuver time. Initial pointing error in z would be expected to add to final pointing error in z. The combination of these expected (prelaunch) errors in z are shown by the dashed line in Fig. 9 and described in Ref. 4. Errors of the y axix can be shown to be dependent not only on the scale factor and uncompensated drift but also that the initial uncertainty (prior to the maneuver) in pointing *about* the x *axis* is a key factor. This can be seen by referring to Fig. 4. A rotation about the x axis at inertial target 1 would result in an orientation error of the maneuver axis and, therefore, the maneuver plane would rotate about the target 1 x axis also. This error source would be the largest for 90-deg maneuver angles and would return to zero for 180-deg maneuvers. Since pointing errors about the x axis at target 1 are a strong function of the guide star separation at this target, the error for 90-deg maneuvers is similarly affected. The combined effect of this error, plus the others as noted above on the y-axis error, are also shown in Fig. 9 for star separations of 3 and 6 deg, respectively.

The errors for 50 maneuvers plotted in Fig. 9 have star separations at the previous target ranging from 3.1 to 6.5 deg, but with only two maneuvers performed with initial star separations greater than 6 deg as labeled. It can be seen that the expected maneuver errors correlate in their general characteristics with those achieved. Errors about z show a trend that increases with maneuver angle, while y-axis errors show a tendency to be larger for midrange maneuvers than for large ones. Since the prelaunch predictions indicated by the lines in Fig. 9 are 1σ values, the achieved maneuver performance is considerably better than the prediction (closer to 3σ for the small sample given) and this is a measure of the conservatism of such predictions.

Star Tracker "Flat-Field" Effects

The use of very small star tracker fields of view has contributed to the high accuracy; however, the small field of view also requires the use of very dim guide stars for a significant number of targets. Stars in the range of 7th to 9th magnitude are frequently used. The need to employ dim stars has resulted in unexpected behavior from the star trackers when operating near the sunlit Earth. Although the star tracker shades are two-stage and are 5 ft long, they are not adequate when operating on dim stars within 26 deg of the bright Earth. Small amounts of reflected light enter the star trackers and raise the background light to levels such that the trackers track everywhere within their field ofview. Commands to break lock at the present track location cause a predetermined jump from the present location. Tracking immediately resumes at the jump location. The tracking occurs not on stars but on background. This behavior has been observed in the ground test of other trackers, but has been presumed due to sky brightness (in air) rather than internal shade reflections.

In the attempt to locate guide stars, the on-board software sends search-continue commands which cause the "jump track" to push the search location across the field of view as shown in Fig. 10. This causes the track location to be pushed across the field of view until it eventually enters the guide star error box. Occasionally this results in passing of the separation tests and improper reference updates occur.

On several occasions, HEAO-2 made unscheduled excursions from normal pointing caused by these improper updates. Eight of these are known for sure, but there may have been other minor occurrences. Typically, the excursions were small, temporary rotations about the x axis that occurred during pointing on or near the lighted Earth. On each occasion, the system was self-correcting, since proper guide stars were reacquired when the Earth moved away from the star tracker boresights during orbital motion.

This behavior was somewhat disturbing to experiment viewing time and it was, therefore, desirable to prevent its occurrence. Also, there was some worry that the observatory might become "lost," i.e., lose attitude reference knowledge such that stars are no longer found in the error boxes. The detailed examination of data that followed these occurrences resulted in the conclusion that improper updates occurred because of star tracker tracking of background rather than true stars. Stray light from the bright Earth raises the background light level such that star trackers track everywhere in the field of view. The characteristics of the tracking data indicated that simple discrimination logic performed on-orbit would eliminate these excursions. The logic prevents updates if the sample-to-sample variation in the data exceeds a given threshold during an observation period. The excursion characteristic has not been observed since the addition of the discrimination logic. Prior to the addition of this logic, updates were performed at 64-s intervals. Since the logic requires examination of star tracker data for 20 successive samples, the additional computations have caused delays that result in a 74-s interval between updates.

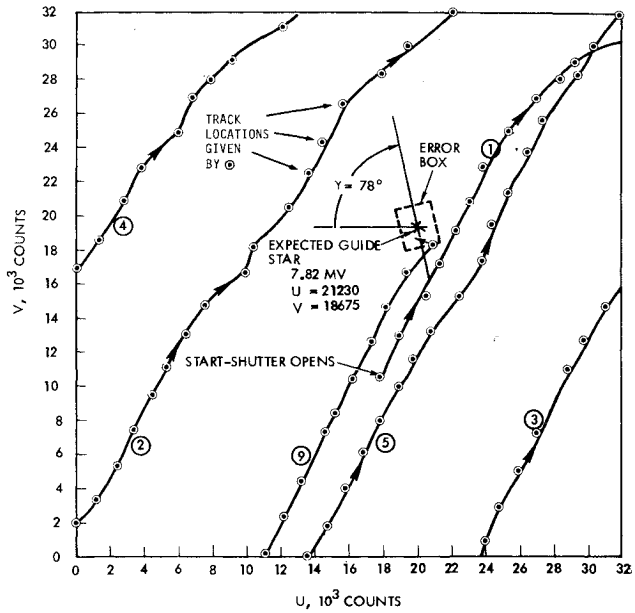

Fig. 10 "C" star tracker track performance characteristic prior to improper update, orbit 111 ACN.

The roll pointing excursions occurred in pairs. The first excursion was apparently cancelled by the second in each event. Detailed star tracker data obtained from two such events have been plotted to describe the data characteristics. The two events shown in Figs. 10 and 11 occurred during real-time passes on orbits 111 ACN and 188 QUI. The time line of the 111 ACN event is given in Table 3.

The track path in the field of view shown in Fig. 10 begins with the opening of the shutter with the tracker immediately tracking at the point marked by the circled dot as shown. Tracking remained at this point for the six minor frames required by delays and the test to determine if the object is within the error box about the expected guide star location. Since the object is not in the box, a search-continue command was issued by the on-board software causing a jump to the second circled dot where immediate tracking began again. The above process was repeated for each circled dot shown. The nominal jump between tracking data points averaged about 2000 counts in V and 1000 counts in U. It should be noted that this is precisely the four search line jump characteristics designed into the star tracker operation to prevent reacquisition of the same star. The apparent effect shown is that a stream of search-continue commands push the track location diagonally across the field of view along the path marked 1. When U or V saturate at maximum value, they are reset to zero and tracking resumes along path 2. On this path, V ultimately saturates, is reset to zero, and push-tracking

Table 3 Time line for 111 ACN event—Nov. 20, 1978

Time	Event
14:27:09Z	Beginning of data.
14:27:19	Star tracker shutters open.
14:28:49	B tracker finds "star" in box at $U=1811$, $V=2836$ after 51 search-continue commands.
14:31:42	C tracker finds a "star" in box at $U=21230$, $V=18675$ after about 150 search-continue commands. "Star" in B tracker has moved to $U=3101$, $V=2847$.
14:32:50	After 64-s time delay, a second update was attempted on the above "stars." However, the "stars" have changed positions relative to each other by hundreds of counts and the separation test fails.
14:34:18	C tracker reacquires a "star" in box.
14:35:39	B tracker acquires "star" in box and separation test fails again. B tracker stays in track in box. C tracker searches to end of data.
14:37:43	End of data.

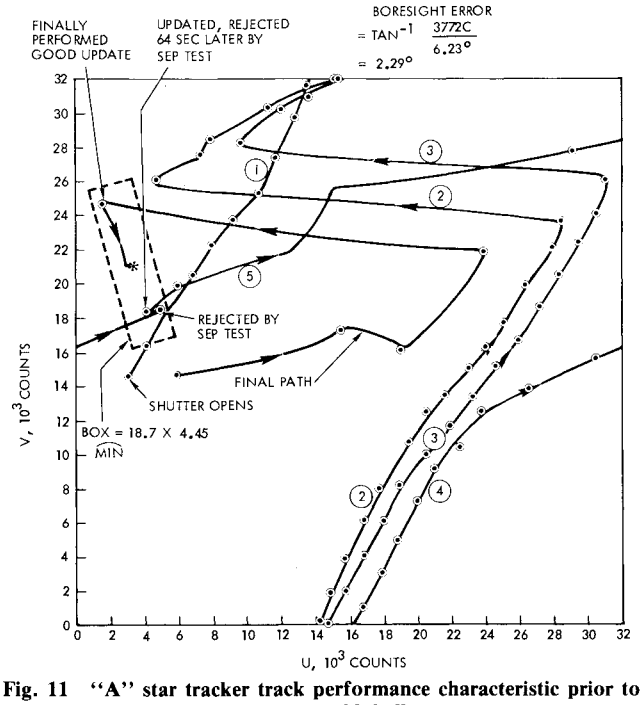

Fig. 11 "A" star tracker track performance characteristic prior to improper and proper updates, orbit 188 QUI.

continues on path 3. This process continued until the ninth trip across the field of view. This path intersected the error box such that tracking occurred within the box. Since the B tracker had previously found an object in its error box, the separation test was performed between these objects and the test passed causing an update. After 64 s, the object in the C tracker moved about 1000 counts in the $-U$ direction and the separation test was performed again for the next update. On this try the separation test failed and tracking resumed. Subsequently, objects were again found in both error boxes and the separation test failed a second time. Searching then continued in the same push-track method until the end of data. The movement of the object by 1000 counts in U during the 64-s update interval corresponds to a drift rate of over 3.5 deg/h. Since this motion is two orders of magnitude greater than observed gyro drift, the tracking is obviously not on stars. It is important to note that the guide stars were of magnitude 7.70 and 7.82 for the ACN 111 case.

The second event occurred on orbit 188 QUI, and had a time line similar to the 111 ACN case shown in Fig. 11. Tracking began immediately (no searching) upon opening of the shutter. Again, local tracking occurred with search-continue commands causing a jump of about 2000 counts in V. The track location path was pushed across the field of view identically as in the ACN 111 case. During the 188 QUI sequence, tracking in the "A" tracker occurred both on background and finally on a guide true star. The guide stars were of magnitude 5.05 and 6.85 mV in the C and A trackers, respectively. During the entire sequence of events, the 5th magnitude star in the C tracker was tracked continuously. The behavior of tracking everywhere in the field of view (wherever pushed by the search continue) was never indicated by this tracker. Since it is known that pointing was from 10 to 30 deg off the Earth during the sequence, it is apparent that the observed tracking characteristic is dependent on the threshold.

The conclusions drawn from the preceding observations are supported by similar observed characteristics on ground test data from similar instruments. If background light levels are high relative to the threshold setting, then star trackers are unable to distinguish the stars from background and track everywhere. If the object is sufficiently brighter than the background, tracking proceeds normally. Since the star tracker shade design on HEAO-2 will allow light to impinge on its first stage at angles up to 26 deg from the boresight, the following conclusions were drawn:

1) Stray light from the bright Earth enters the star tracker raising the background intensity.

2) If the background is sufficiently bright, the star trackers track everywhere in their field of view.

3) When tracking background light, the on-board software search-continue commands push the track location into the error box, occasionally performing erroneous updates.

4) Star tracker shade characteristics do not allow proper tracking of 7th to 8th magnitude stars within 26 deg of the bright Earth.

Examination of tracking data for both background tracking and star tracking reveals important differences in the variations from minor frame to minor frame. Tracking of bright stars (5 mV) shows only 2-3 counts of variation from one minor frame to the next. Count variations increase somewhat for dim stars (7-8 mV, threshold 5) to about 10 counts peak, with rare occurrences of larger excursions. On the other hand, background tracking invariably shows a search of not more than one minor frame (immediate track) with count variations typically in the range 20 to 50 with frequent excursions of hundreds of counts.

The previous observations resulted in derivation of a simple method for implementation in the on-board flight program to eliminate improper updates. The method consists of examining the U,V count changes each sample period. The change must not exceed a certain number (selected at 15 counts) and this test must be passed for all U,V data for an entire observation period (20 successive samples selected) before an update is allowed. This technique uses tracker counts that have been corrected for spacecraft motion rather than raw tracker data.

Conclusions

The on-orbit operational experience with the HEAO-2 observatory control system indicates that the design concepts have been confirmed and that celestial pointing and maneuvering accuracy capabilities have significantly surpassed their design requirements. The knowledge of improvement of capabilities over requirements could be utilized to advantage in the development of observation profiles and to simplify the target selection process. The inherent flexibility provided by the on-board digital processor has

provided a valuable capability to overcome unforeseen characteristics and to modify operational capabilities. This allows optimization of performance and simplification of the ground operations interface.

Acknowledgments

The development program for the three HEAO spacecraft was initiated in July 1974 under management of the NASA Marshall Space Flight Center, Contract NAS8-28300. The HEAO-2 experiments are operated by a consortium of experiments involving scientists from five organizations including the Smithsonian Astrophysical Observatory (SAO), Massachusetts Institute of Technology (MIT), Goddard Space Flight Center (GSFC), and Columbia Astrophysics Laboratory (CAL). The principal investigator and scientific director of the consortium is Dr. Riccardo Giacconi of SAO.

The authors express their appreciation to the Goddard Space Flight Center for cooperation and support in providing data on the HEAO-2 observatory operations, and to Dr. Steven Murray of the Smithsonian Astrophysical Observatory for the many discussions of the control system performance.

The success of the HEAO program has occurred because of the many dedicated people at the Marshall Space Flight Center and at TRW. Special acknowledgment is afforded to those who have contributed so very much to the attitude control subsystem success.

References

[1] Neighbors, A.K., Doolittle, R.F., and Halpern, R.E., "High Energy Astronomy Observatories," Paper 77-282, AIAA Annual Meeting, Washington, D.C., Jan. 1977.

[2] Wojtalik, F.S., "High Energy Astronomy Observatory Program," Seventh IFAC World Congress, Helsinki, Finland, June 1978.

[3] Hoffman, D.P. and McElroy, T.T., "HEAO Attitude Reference Design," Paper AAS 78-120, AAS Annual Rocky Mountain Guidance and Control Conference, Keystone, Colo., March 1978.

[4] Hoffman, D.P. and Berkery, E.A., "On-Orbit Experience with the HEAO-1 Attitude Control Subsystem," AIAA Paper 78-1263, *AIAA Guidance and Control Conference,* Palo Alto, Calif., Aug. 1978.

[5] Farrenkopf, R.L. and Hoffman, D.P., "Guide Star Targeting Success for the HEAO-B Observatory," AIAA Paper 77-1040, *AIAA Guidance and Control Conference,* Aug. 1977.

[6] Henry, P., "The X-Ray Eyes of Einstein," *Sky and Telescope,* June 1979.

From the AIAA Progress in Astronautics and Aeronautics Series . . .

VISCOUS FLOW DRAG REDUCTION—v. 72

Edited by Gary R. Hough, Vought Advanced Technology Center

One of the most important goals of modern fluid dynamics is the achievement of high speed flight with the least possible expenditure of fuel. Under today's conditions of high fuel costs, the emphasis on energy conservation and on fuel economy has become especially important in civil air transportation. An important path toward these goals lies in the direction of drag reduction, the theme of this book. Historically, the reduction of drag has been achieved by means of better understanding and better control of the boundary layer, including the separation region and the wake of the body. In recent years it has become apparent that, together with the fluid-mechanical approach, it is important to understand the physics of fluids at the smallest dimensions, in fact, at the molecular level. More and more, physicists are joining with fluid dynamicists in the quest for understanding of such phenomena as the origins of turbulence and the nature of fluid-surface interaction. In the field of underwater motion, this has led to extensive study of the role of high molecular weight additives in reducing skin friction and in controlling boundary layer transition, with beneficial effects on the drag of submerged bodies. This entire range of topics is covered by the papers in this volume, offering the aerodynamicist and the hydrodynamicist new basic knowledge of the phenomena to be mastered in order to reduce the drag of a vehicle.

456 pp., 6×9, illus., $25.00 Mem., $40.00 List

TO ORDER WRITE: Publications Dept., AIAA, 1290 Avenue of the Americas, New York, N.Y. 10104